

An additional soft X-ray component in the dim low/hard state of black hole binaries

C. Y. Chiang^{1*}, Chris Done¹, M. Still^{2,4}, and O. Godet³

¹*Department of Physics, University of Durham, South Road, Durham DH1 3LE, UK*

²*Mullard Space Science Laboratory, Dorking, Surrey, UK*

³*X-ray and Observational Astronomy Group, Department of Physics and Astronomy, University of Leicester, LE1 7RH, UK*

⁴*NASA Ames Research Center, Moffett Field, CA 93045, USA*

Submitted to MNRAS

ABSTRACT

We test the truncated disc models using multiwavelength (optical/UV/X-ray) data from the 2005 hard state outburst of the black hole SWIFT J1753.5-0127. This system is both fairly bright and has fairly low interstellar absorption, so gives one of the best datasets to study the weak, cool disc emission in this state. We fit these data using models of an X-ray illuminated disc to constrain the inner disc radius throughout the outburst. Close to the peak, the observed soft X-ray component is consistent with being produced by the inner disc, with its intrinsic emission enhanced in temperature and luminosity by reprocessing of hard X-ray illumination in an overlap region between the disc and corona. This disc emission provides the seed photons for Compton scattering to produce the hard X-ray spectrum, and these hard X-rays also illuminate the outer disc, producing the optical emission by reprocessing.

However, the situation is very different as the outburst declines. The optical is probably cyclo-synchrotron radiation, self-generated by the flow, rather than tracing the outer disc. Similarly, limits from reprocessing make it unlikely that the soft X-rays are directly tracing the inner disc radius. Instead they appear to be from a new component. This is seen more clearly in a similarly dim low/hard state spectrum from XTE J1118+480, where the $10\times$ lower interstellar absorption allows a correspondingly better view of the UV/EUV emission. The very small emitting area implied by the relatively high temperature soft X-ray component is completely inconsistent with the much larger, cooler, UV component which is well fit by a truncated disc. We speculate on the origin of this component, but its existence as a clearly separate spectral component from the truncated disc in XTE J1118+480 shows that it does not simply trace the inner disc radius, so cannot constrain the truncated disc models.

Key words: X-rays: binaries – accretion, accretion discs

1 INTRODUCTION

The accretion disc in black hole binary systems (BHB) is unstable at the point where Hydrogen goes from being predominantly neutral to ionised. This gives rise to dramatic, transient outbursts in which the reservoir of material built up in the outer disc during quiescence can accrete down onto the black hole. The peak luminosity of the outburst is set by the mass in the quiescent disc and the time taken for this to accrete. Both these depend on the size of the disc taking part in the outburst, which is set by the binary separation. Hence there is a link between orbital period and peak luminosity, with short period systems showing smaller peak outburst lu-

minosities (King & Ritter 1998; Shahbaz et al. 1998; Lasota 2001; Done, Gierliński & Kubota 2007 hereafter DGK07).

The peak luminosity determines the number of spectral states which are seen during the outburst. Systems with peak luminosity below $\sim 0.1L_{Edd}$ remain in the low/hard state (LHS), where the energy output peaks at ~ 100 keV. Brighter systems instead show a distinct transition to a much softer thermal dominated state (TDS, also termed a high/soft state) which peaks at ~ 1 keV, while the brightest systems can also show a very high state (VHS, alternatively steep power law state). These dramatic changes in the spectrum are correlated with equally dramatic changes in the rapid variability properties (see e.g. McClintock & Remillard 2006) and the jet (Fender, Belloni & Gallo 2004), implying distinct changes in the nature and geometry of the accretion flow. These can be plausibly explained if there is a hot, optically thin, geometrically

* E-mail: chia-ying.chiang@durham.ac.uk

thick solution to the accretion flow equations at low luminosities (Shapiro, Lightman & Eardley 1976; Narayan & Yi 1995). This can be put together with a cool, optically thick, geometrically thin disc (Shakura & Syunyaev 1973) in the truncated disc/hot flow model where the disc progressively replaces more of the inner hot flow as the mass accretion rate increases. The distinct hard/soft spectral transition then marks the point at which the cool disc extends down to the last stable orbit, replacing all the hot flow (Esin, McClintock & Narayan 1997; DGK07).

Such models make a clear prediction that the inner radius of the cool disc should recede as the LHS drops in luminosity. This can in principle be tested using the colour temperature and luminosity of the cool disc component to estimate its radius (e.g. Poutanen, Krolik & Ryde 1997; Shrader & Titarchuk 1999). However, such observations are complicated by the fact that the disc is at low temperature at low luminosities, ~ 0.3 keV for a $10M_{\odot}$ black hole at $0.02L_{Edd}$, even if the disc extends down to $6R_g$ (where $R_g = GM/c^2$). Such low energy X-rays cannot be seen with the 3 keV bandpass limit of *RXTE*, the satellite which has accumulated the most BHB data to date (Done & Gierliński 2003; Dunn et al. 2009). CCD observations can extend the bandpass down to lower energies, but these are still not straightforward to interpret as the disc is not the dominant spectral component in this state. Instead, the hard X-ray emission dominates the spectrum, so irradiation can change the disc temperature (Gierliński, Done & Page 2008, hereafter GDP08), while the disc luminosity can be underestimated due to photons which are Compton upscattered into the hard X-ray spectrum (Makishima et al. 2008). This component is still not easy to study even with CCD detectors since low energy X-rays are absorbed by interstellar gas. Most BHB are in the galactic plane so have gas columns of $N_H \geq 10^{22} \text{ cm}^{-2}$ which effectively block emission below 1 keV.

However, there are a few black holes which have intrinsically much lower columns which have been observed with CCD detectors, namely XTE J1118+480: $N_H \sim 1.1 \times 10^{20} \text{ cm}^{-2}$, XTE J1817-330: $1.1 \times 10^{21} \text{ cm}^{-2}$ and SWIFT1753.5-0127: $2 - 3 \times 10^{21} \text{ cm}^{-2}$ (Cabanac et al. 2009). XTE J1118+480 has only snapshot spectra available (Hynes et al. 2000; Esin et al. 2001; Frontera et al. 2001; 2003), but both SWIFT1753.5-0127 and XTE J1817-330 were well sampled throughout their outbursts by the *Swift* satellite. However, XTE J1817-330 is a long period system, so spends most of its time in the disc dominated state, with only two, rather faint, LHS spectra at the end of its outburst. Thus the short period LHS outburst of SWIFT1753.5-0127 is the best candidate to study the disc evolution in the LHS. Here we analyse these data with sophisticated models to describe the behaviour of the X-ray irradiated disc (GDP08; Gierliński, Done & Page 2009, hereafter GDP09) to constrain its inner radius as the outburst declines.

2 DATA REDUCTION

2.1 *Swift*

We use publicly available *Swift* data from SWIFT J1753.5-0127 taken during the period from July 2005 to July 2007. We extracted both X-ray telescope (XRT) and UVOT data. All of our XRT data was in Windowed Timing mode, and we extracted source counts using a circle with radius of 20 pixels. Background was taken from an off source region using a circle of the same size. However, the source was very bright during the peak of the outburst, and some of the datasets were piled up as the count rate was

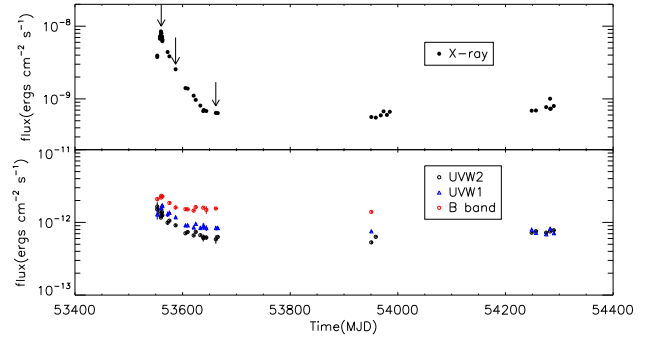


Figure 1. The top panel shows the evolution of the observed flux in the *Swift* XRT band, while the lower panel shows the simultaneous UVOT data (in UVW1, UVW2 and B filters, where available).

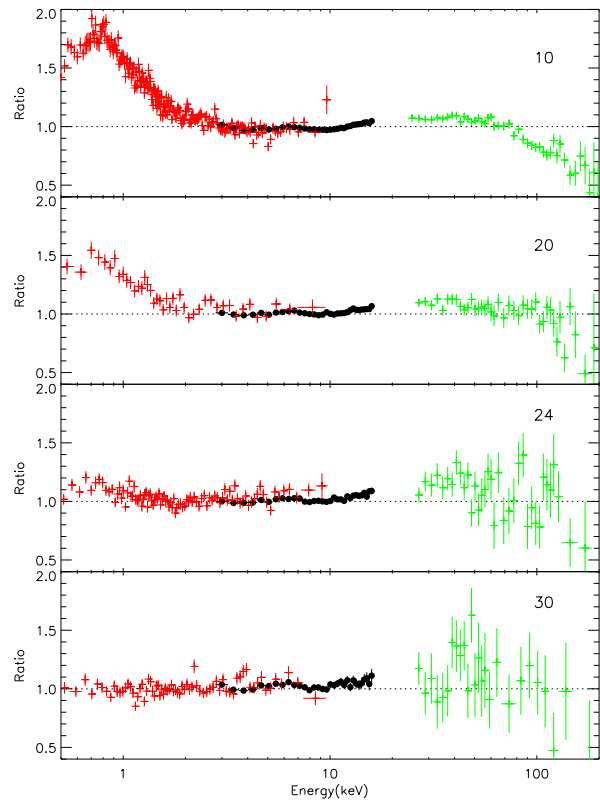


Figure 2. The ratio of the X-ray data (red:XRT, black:PCA, green:HEXTE) to an absorbed power law model fit to the 2-4 and 7-10 keV ‘continuum dominated’ bands for spectra taken from the peak (10) through to the end of the decline (30) as marked by arrows on Fig 1. At the peak is clear that the continuum spectrum strongly declines above 70 keV, indicating that the electron temperature of the thermal Comptonisation is low enough to be seen. There is also a strong additional soft component at low energies, most probably from the accretion disc, together with a small features around the iron line and edge, indicating reflection of the continuum from the accretion disc. As the outburst declines, the electron temperature increases, so the high energy break can no longer be seen, and the soft X-ray emission drops dramatically in strength.

Table 1. The table details the datasets we use from *Swift* and *RXTE*. We refer to the combined spectrum by the last two numbers of its *Swift* obsID. The remaining columns give the QPO frequency from fitting the *RXTE* power spectrum, followed by the results for fitting the 0.5-200 keV X-ray data with a `wabs*(diskbb+thCompml)` model. We fix the absorption to $0.2 \times 10^{22} \text{ cm}^{-2}$, and assume reflection is from neutral, solar abundance material inclined at 60° . We tie the seed photons for Comptonisation to the disc temperature in these fits, but then also show the difference in χ^2 for removing the disc and fixing the seed photon energy for the Compton scattering to 0.1 eV

Number	<i>Swift</i>	<i>RXTE</i>	QPO (Hz)	$kT_{disc}(keV)$	N_{dbb}	Γ	$\Omega/2\pi$	N_{pl}	χ^2/ν	$\Delta\chi^2$
00	00143778000	91094-01-01-00	0.64 ± 0.01	0.22 ± 0.01	47557	1.80 ± 0.02	$0.34^{+0.10}_{-0.13}$	0.58	712/713	699
03	00030090003	91094-01-01-04	0.83 ± 0.01	$0.25^{+0.00}_{-0.01}$	63806	$1.86^{+0.00}_{-0.02}$	$0.35^{+0.05}_{-0.08}$	1.06	544/548	1024
04	00030090004	91423-01-01-04	0.91 ± 0.01	$0.24^{+0.00}_{-0.01}$	66358	1.86 ± 0.01	0.27 ± 0.06	1.06	870/757	1503
07	00030090007	91094-01-02-01	$0.75^{+0.01}_{-0.02}$	$0.24^{+0.01}_{-0.00}$	69967	$1.83^{+0.02}_{-0.01}$	$0.36^{+0.04}_{-0.08}$	1.16	702/679	1112
06	00030090006	91094-01-02-01	“	$0.24^{+0.00}_{-0.01}$	83839	$1.82^{+0.02}_{-0.01}$	$0.32^{+0.08}_{-0.07}$	1.26	868/762	1674
10	00030090010	91094-01-02-00	$0.72^{+0.00}_{-0.01}$	$0.25^{+0.00}_{-0.01}$	70377	$1.82^{+0.01}_{-0.02}$	$0.33^{+0.03}_{-0.04}$	1.17	752/726	2192
08	00030090008	91094-01-02-00	“	0.28 ± 0.02	36514	1.81 ± 0.01	$0.28^{+0.04}_{-0.04}$	0.86	275/273	232
09	00030090009	91094-01-02-00	“	$0.24^{+0.01}_{-0.00}$	73119	$1.81^{+0.01}_{-0.01}$	0.28 ± 0.05	1.17	873/784	2955
11	00030090011	91094-01-02-02	0.70 ± 0.01	0.25 ± 0.02	59219	1.81 ± 0.01	0.29 ± 0.06	1.02	333/320	250
12	00030090012	91094-01-02-02	“	$0.23^{+0.01}_{-0.00}$	79673	1.81 ± 0.01	$0.29^{+0.05}_{-0.06}$	1.09	860/746	1898
13	00030090013	91094-01-02-02	“	$0.23^{+0.01}_{-0.00}$	75104	1.81 ± 0.01	0.30 ± 0.06	1.08	622/633	1134
15	00030090015	91094-01-02-03	0.63 ± 0.01	$0.23^{+0.00}_{-0.01}$	69620	1.79 ± 0.01	$0.31^{+0.07}_{-0.06}$	0.99	818/743	1231
16	00030090016	91094-01-02-03	“	0.25 ± 0.01	49618	1.79 ± 0.01	$0.31^{+0.06}_{-0.07}$	0.94	717/655	1030
18	00030090018	91423-01-03-06	0.47 ± 0.01	$0.23^{+0.01}_{-0.02}$	42447	1.73 ± 0.01	0.24 ± 0.06	0.64	396/435	347
19	00030090019	91423-01-04-02	$0.45^{+0.00}_{-0.01}$	0.22 ± 0.01	39291	1.72 ± 0.01	$0.28^{+0.07}_{-0.06}$	0.57	626/646	732
20	00030090020	91423-01-06-00	0.29 ± 0.01	$0.23^{+0.01}_{-0.02}$	17415	$1.67^{+0.02}_{-0.01}$	$0.20^{+0.07}_{-0.09}$	0.36	433/460	178
21	00030090021	91423-01-08-02	-	0.22 ± 0.02	9122	1.65 ± 0.03	$0.19^{+0.16}_{-0.17}$	0.21	514/518	50
23	00030090023	91423-01-10-00	-	0.17 ± 0.02	14876	$1.65^{+0.01}_{-0.02}$	$0.16^{+0.05}_{-0.09}$	0.18	635/659	32
24	00030090024	91423-01-11-00	-	$0.16^{+0.02}_{-0.03}$	16135	$1.67^{+0.01}_{-0.02}$	$0.24^{+0.11}_{-0.13}$	0.16	602/631	19
26	00030090026	91423-01-13-00	-	$0.17^{+0.05}_{-0.10}$	4629	$1.63^{+0.02}_{-0.04}$	$0.13^{+0.14}_{-0.13}$	0.11	559/562	4
30	00030090030	91423-01-16-01	-	$0.04^{+0.05}_{-0.03}$	934	$1.64^{+0.01}_{-0.02}$	$0.09^{+0.14}_{-0.09}$	0.11	559/592	3
31	00030090031	91423-01-17-00	-	$0.13^{+0.04}_{-0.12}$	13157	$1.63^{+0.02}_{-0.03}$	$0.14^{+0.16}_{-0.14}$	0.10	576/508	3

above 100 counts s^{-1} . We determined the size of the central piled up region by excluding progressively larger radii regions until the spectra stopped softening at high energies. This gave an exclusion region of 3 pixels for brightest observations, and 2 pixels for more moderately piled up data. The data was grouped to 20 counts s^{-1} , and fit between 0.5-10 keV.

The evolution of the observed (i.e. not corrected for interstellar absorption) flux in the X-ray (upper) and UV (lower) bands is plotted in Fig. 1. We derive the flux by integrating the absorbed model fit over 0.5-10 keV for the X-rays. For UV data, we find energy band for each filter and define the effective bandpass to be between the energies determined by FWHM (5.6×10^{-3} to 7.45×10^{-3} keV for UVW2 filter, 4.2×10^{-3} to 5.45×10^{-3} keV for UVW1 filter, and 2.55×10^{-3} to 3.2×10^{-3} keV for B filter).

The observations fall into 3 clearly distinct time segments. The first covers the outburst rise and decline, after which the flux remains fairly constant. Hence in this paper we concentrate on this first data group, in order to track the evolution of the disc during the flux decline.

2.2 *RXTE*

The *RXTE* satellite also followed the 2005 outburst. We use the standard extraction techniques with the bright source background to derive PCA spectra from all layers of detector 2, adding 1 percent systematic error and use these data from 3-16 keV. We also extract Standard 1 power spectra over the full 2-60 keV bandpass for intervals of 256 s, and fit these with multiple Lorentzian com-

ponents in order to determine the QPO frequency. These are given in Table 1.

We extract HEXTE data from cluster 0 and use these over the energy range 25-200 keV. We select the subset of *Swift* and *RXTE* data which are taken within one day of each other. This gives a total of 27 observations which have quasi-simultaneous coverage of the optical/UV/X-ray/hard X-ray spectrum. Table 1 details these composite spectra.

3 DISC PLUS COMPTONISATION PLUS REFLECTION

3.1 X-ray data

We first concentrate on the X-ray data alone, and show the different components present in the spectrum. We fit a power law to the ‘continuum dominated’ bands at 2–4 keV and 7–10 keV, and then show a ratio of the data to this model over the entire bandpass (assuming absorption fixed at the galactic column of $N_H = 0.2 \times 10^{22} \text{ cm}^{-2}$). Fig. 2 shows this at different points along the outburst (marked by arrows in Fig. 1), from the peak to the end of the decline. Close to the peak, the continuum clearly has a rollover at high energies, so is most likely due to thermal Comptonisation. There is also clearly an additional soft X-ray component, which decreases in strength as the outburst declines. However, there are also more subtle features seen in the high signal-to-noise PCA data, with a small excess around the iron line, followed by a slight dip and subsequent rise to 20 keV. This is characteristic of reflection

Thus we use a model including a disc to produce the soft X-ray component, thermal Comptonisation of these disc

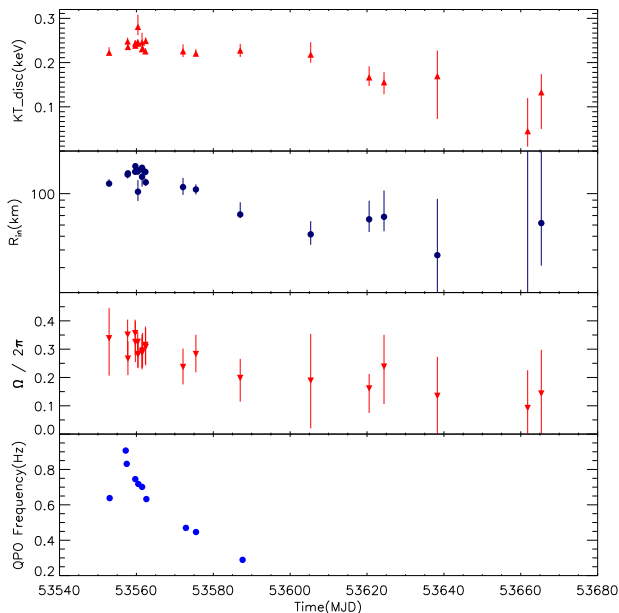


Figure 3. The plot shows the results of the disc temperature, inner radius and reflection evolution obtained from the `diskbb+thComp` model. The value of inner radius were derived from the `diskbb` normalisation assuming an inclination of 60° and distance of 5.4kpc. As these are poorly known, the absolute value of the radius is not well constrained. However, trends should be robust, and clearly the derived inner radius remains constant or mildly decreases during the outburst. This is in sharp contrast to the expected increase from truncated disc models. Reflection (third panel) and the QPO frequency (lower panel, see also Table 1), on the other hand, decreases when leaving the peak, as expected if the disc is receding.

seed photons to produce the hard continuum, and reflection of the hard continuum from the surface of the disc. We use the THCOMP model to describe the Comptonisation, developed and tested by Zdziarski, Poutanen & Johnson (2000), extended to include its reflected continuum and self-consistent line emission by Życki, Done & Smith (1999). We assume that the reflecting material is neutral, with solar abundances and inclined at 60° . We fix the galactic absorption column at $N_H = 0.2 \times 10^{22} \text{ cm}^{-2}$ corresponding to an $E(B - V) = 0.34$ (Cadolle Bel et al. 2007). The results for each spectrum are detailed in Table 1. We assess the significance of the detected disc emission by removing the disc from the model, and fixing the seed photon temperature instead at 0.1 eV. This results in a loss of 2 degrees of freedom, so the disc is only significant at greater than 99 per cent confidence for $\Delta\chi^2 > 4.61$. Thus all the spectra apart from the final 3 (26, 30 and 31) strongly require the presence of an additional soft component. We similarly assess the significance of reflection (driven mostly by the presence of the iron line) and find that it is required in all the datasets apart from the final 3.

Fig. 3 shows the derived disc temperature and radius (see Table 1). The disc radius *decreases* as the outburst progresses (see also Cabanac et al. 2009), in apparent conflict with the truncated disc model where the inner disc should progressively recede during the LHS decline. Yet the amount of reflection decreases, as expected if the disc is receding. Additionally, the low frequency QPO seen in the variability power spectrum drops dramatically, again as expected if the truncation radius sets the QPO frequency and is increasing (DKG07). Thus while the behaviour of the reflected

emission and QPO fit the truncated disc models, the behaviour of the soft X-ray component does not.

3.2 Optical data

We show these X-ray model fits extrapolated down to the optical/UV data and corrected for the effects of interstellar absorption. Fig. 4a shows this for the outburst peak (10). This clearly shows that extrapolating the hard X-ray power law spectrum down in energy *overpredicts* the optical/UV data. This implies that the hard X-ray spectrum must break at UV/soft X-ray energies, supporting our modeling of it as due to Comptonisation of seed photons from the accretion disc. However, extrapolating the soft X-ray disc emission *underpredicts* this emission, making it clear that intrinsic gravitational energy release in the disc is insufficient to produce the observed optical/UV data.

In general, the optical can include additional contributions from reprocessed emission from hard X-ray illumination of the outer disc, as well as contributions from the jet and the companion star (e.g. Russell et al. 2006). However, SWIFT J1753.5-0127 is a short period, low mass X-ray binary, so the companion star must faint. Instead we try to quantify the jet contribution from observed radio flux of $\sim 2.1 \text{ Jy}$ at 1.7 GHz (Fender et al. 2005). We show the extrapolation of this up through our optical/UV/X-ray bandpass assuming a flat spectrum (black line on Fig. 4a). This is a factor ~ 3 below the observed optical flux, but this is the maximum possible jet contribution as its spectrum should break where it becomes optically thin. It seems most likely that this break is at IR frequencies (Markoff et al. 2001; Gallo et al. 2007) so the jet is also probably negligible in the optical/UV for these data. Thus X-ray reprocessing from hard X-ray illumination of the outer disc seems the most likely origin for the optical/UV flux (van Paradijs 1996).

There are additional radio observations from midway down the outburst decline (Cadolle Bel et al. 2007). Fig. 4b shows this radio emission, extrapolated as above, onto spectrum 20, the dataset closest in time to the radio observations. Again, the optical/UV points are not fit by either the hard X-ray power law extrapolated down (though this time the mismatch is not so large), or by the radio emission extrapolated up, or by the disc inferred from the soft X-ray component, as also shown in Cadolle Bel et al. (2007).

Fig. 4c shows a spectrum from the end of the outburst (30), where there are no radio observations. The disc emission fit to the soft X-ray component is now very weak and cool, and its extrapolation down to the optical lies dramatically below the observed optical/UV emission. However, the optical/UV emission does lie remarkably close to the extrapolated hard X-ray flux in these low-luminosity data.

We quantify this by calculating the factor by which the disc component underpredicts the observed flux in the UVW1 filter ('UV excess': GDP09) in each spectrum. We also calculate a 'UV deficit', which is the factor by which the Comptonisation model *overpredicts* the flux in the UVW1 filter if its seed photons put at 0.1 eV rather than fixed to the disc temperature. Such low energy seed photons may be produced by cyclo-synchrotron emission by the same thermal electrons which produce the Compton scattered emission interacting with the tangled magnetic field in the hot flow itself (Narayan & Yi 1995; Di Matteo, Celotti & Fabian 1997; Wardziński & Zdziarski 2000). Fig. 5 shows how these evolutions during the outburst. This confirms the results seen in the three individual spectra discussed above. The 'UV excess' (red triangles) increases strongly with time, as the soft X-ray disc component makes less and less contribution to the UV flux. The disc is not signifi-

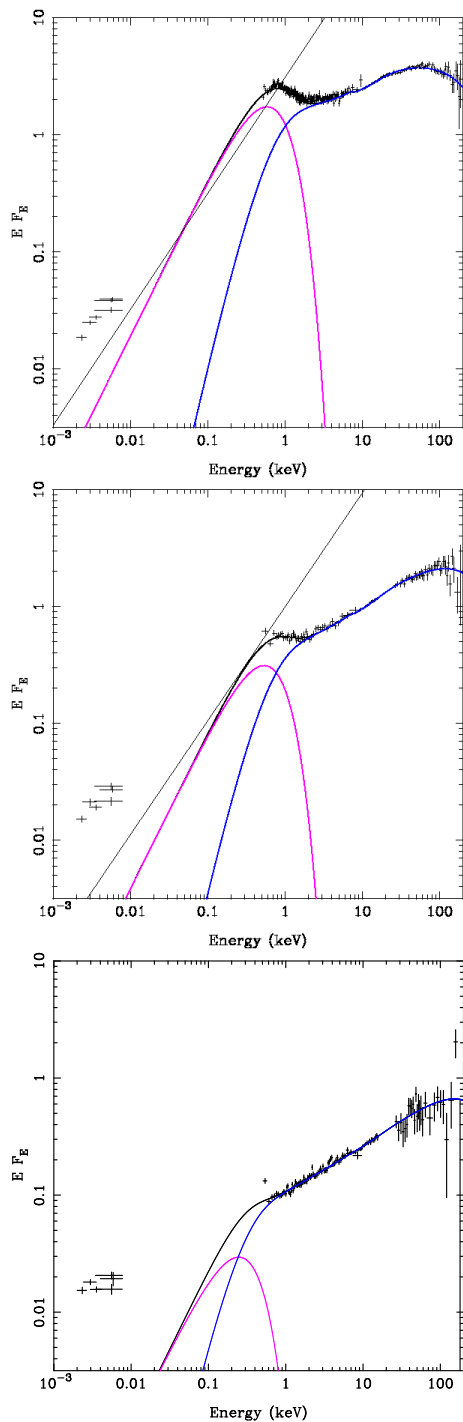


Figure 4. The unabsorbed data and X-ray model fit (`diskbb + thComp1`) at the outburst peak (top panel, spectrum 10), midway down the decline (middle panel, spectrum 20) and in the outburst tail (lower panel, spectrum 30). The magenta and blue components are disc emission and Comptonisation in corona, respectively.

cantly detected in the final three spectra, but the trend in UV excess is already clearly apparent. Conversely, the UV deficit (blue squares) decreases, and is roughly consistent with the observed UV flux from spectrum 21 onwards.

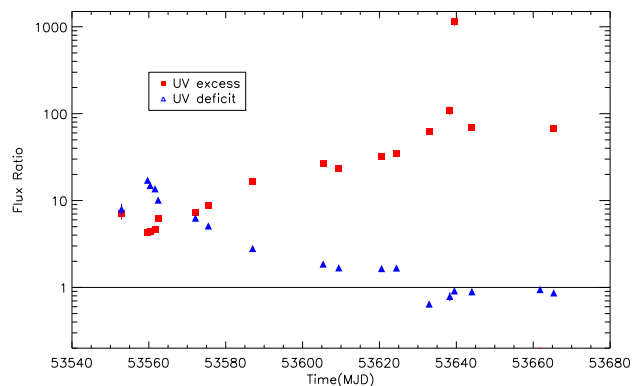


Figure 5. The red squares show the evolution of UV excess i.e. the observed UVW1 flux divided by the UVW1 flux predicted by the model fit to the soft X-ray disc. This always underpredicts the observed UVW1 emission, by an amount that increases as the source fades. The soft X-ray disc component is not significant in the final 3 points but the trend is already clear even without these data. The blue triangles show the 'UV deficit' i.e. the ratio of model to observed flux in the UVW1 filter predicted from extrapolating the `thComp1` continuum down into the optical assuming the seed photons are at 0.1 eV rather than from the disc. Close to the peak of the outburst this UV deficit is large, showing that the X-rays over-predict the UV flux. Conversely, towards the end of the outburst, the UV data lie very close to the extrapolation of the hard X-ray flux.

4 IRRADIATED DISC MODEL

We first look at the possibility that irradiation of the disc is responsible for all the issues highlighted in the previous section. Irradiation of the inner disc changes its derived temperature and radius compared to that derived from fitting purely gravitational energy release models of the disc (GDP08). Similarly, irradiation of the outer disc can also increase the optical/UV emission from that expected from an unilluminated disc (van Paradijs 1996; GDP09)

We use a slightly modified version of the `diskir` model of GDP08 so that the disc temperature and normalisation are set by the physical variables of the mass, distance, mass accretion rate and inner and outer radii. This has the advantage that the outer radius is set in terms of physical units, rather than relative to the (possibly changing) inner radius as in `diskir`. We parameterise the inner and outer radii in terms of $R_g = GM/c^2$, and leave the inner disc radius, R_d as a free parameter in the fits. We fix the mass and distance at the best (though poorly constrained) estimates of $12 M_\odot$ and 5.4 kpc, respectively (Zurita et al. 2008).

This model uses the `DISKBB` parameterisation of disc temperature with radius i.e. $T \propto r^{-3/4}$ (Mitsuda et al. 1984), so does not include a stress-free inner boundary condition or colour temperature correction. If the disc is truncated then the lack of stress-free inner boundary condition is probably more appropriate, but the colour temperature correction, f_{col} , is still an issue. The derived value of the inner radius is then underestimated by a factor $f_{col}^2 \sim 2.9$ for $f_{col} \sim 1.7$ (Kubota, Makishima & Ebisawa 2001). However, the main aim of our spectral fitting is to track *changes* in the value of the inner disc radius, as its absolute value depends on the poorly known system parameters. The key aspect of the truncated disc model which we are testing is the prediction that the truncation radius increases as the spectrum hardens during the de-

cline. Thus we are focussing on the relative values of the inner disc radius during the decline.

The outer radius should remain constant, as should the absorption (but see Cabanac et al. 2009) so we constrain these by simultaneously fitting three datasets from various points in the outburst with the modified `diskir` model, together with X-ray absorption parameterised by `wabs` and UV reddening by `redden`. Assuming standard gas to dust ratios allows us to tie $E(B - V) = 1.5 \times N_H / 10^{22}$ (GDP08). This gives a best fit at $N_H = 2.1 \times 10^{21} \text{ cm}^{-2}$ and $R_{out} = 10^{5.25} R_g$, which are fixed to these values in all fits hereafter.

4.1 Evolution of the irradiated disc model parameters

We fit this model to all the *Swift-RXTE* datasets. Guided by previous low/hard state data (Poutanen, Krolik & Ryde 1997; GDP08), we fix the radius of the irradiated portion of the inner disc at $1.1 \times R_d$. Fig. 6 shows the evolution of the source parameters in this model. The top panel gives the bolometric flux, which varies by an order of magnitude. This is dominated by the hard X-ray component, whose spectral photon index (second panel) decreases from 1.8 to 1.6 during the first section of the decline, and then stabilizes at this value hereafter. The source did not make a transition to the high/soft or even intermediate state, but remained in the hard state throughout the outburst.

The disc spectrum forms a component which connects the soft X-ray rise to the optical emission in this model. Part of this is powered by gravitational energy release, and the inferred mass accretion rate through the disc decreases by more than 2 orders of magnitude during the decline (third panel). Thus the ratio of the hard X-ray flux to this inferred intrinsic disc flux increases by an order of magnitude (fourth panel).

The intrinsic gravitational energy of the disc is augmented by thermalisation of the irradiating flux on the inner disc. The fraction of the hard X-ray spectrum which illuminates the *inner* disc and is thermalised basically decreases during the decline (fifth panel), as expected if the inner edge of the disc is receding. Similarly, the amount of hard X-ray reflection also declines (sixth panel). Conversely, the fraction of hard X-rays which thermalise in the *outer* disc increases by almost an order of magnitude (seventh panel). The final panel shows the disc inner radius. This is plainly consistent with a more or less constant value, at $\sim 10 R_g$, (corresponding to $\sim 30 R_g$ after a colour temperature correction) although the error bars become large at later stages of the decline. Fig. 7a-c show the corresponding fits to the data of Figs. 4a-c for this model.

4.2 Inferred mass accretion rate

We can use these derived parameters to explore how the mass accretion rate through the disc compares to that required to power the hard X-rays. We calculate the mass accretion rate of the corona by:

$$L_c = \frac{\eta_{corona}}{\eta_{disc}} \frac{GM\dot{m}_c}{2R_c},$$

where $\eta_{corona}/\eta_{disc}$ is the relative efficiency of converting mass to radiation in a coronal flow which extends down to R_c versus that in a disc extending down to the same radius. However, the disc itself only extends down to a radius R_d so its luminosity from gravitational energy release alone is $L_d = \frac{1}{2}GM\dot{m}_d/R_d$. Thus

$$\frac{L_c}{L_d} = \frac{\eta_{corona}}{\eta_{disc}} \frac{\dot{m}_c}{\dot{m}_d} \frac{R_d}{R_c}.$$

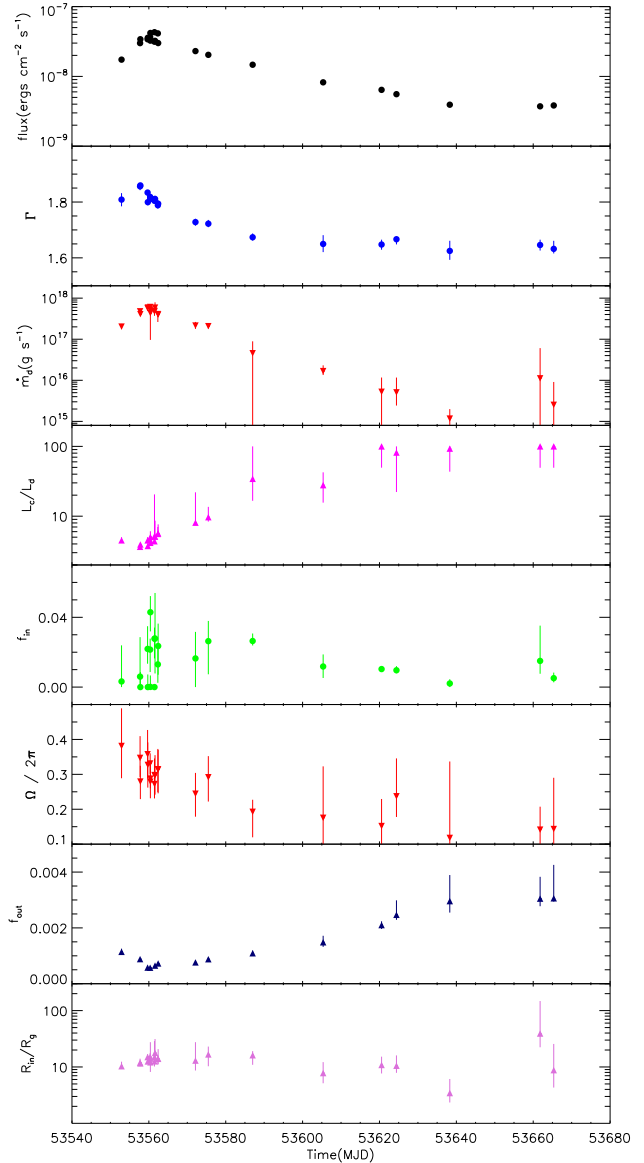


Figure 6. Evolution of an irradiated disc model fit to the optical/UV/X-ray spectrum. The top panel shows the bolometric flux, taken from the unabsorbed model integrated between 0.001–100 keV. This drops by a factor of 10 during the outburst, close to that seen from the X-ray emission alone in Fig. 1. The second panel shows the hard X-ray spectral index, which hardens from 1.8 to 1.6. The third panel shows the mass accretion rate \dot{m}_d required to power the intrinsic (gravitational) emission from the disc luminosity, $L_d = GM\dot{m}_d/2R_d$. This drops by nearly two orders of magnitude, so the ratio of this to hard X-ray luminosity in the corona L_c/L_d increases by a factor 10 (fourth panel). The intrinsic disc luminosity is enhanced by irradiation of the inner disc by the hard X-ray corona. The fraction of irradiation required drops during the decline (fifth panel) as does the amount of (neutral) reflected emission (sixth panel). The seventh panel shows the fraction of the bolometric flux which is required to thermalise in the outer disc in order to make the observed optical/UV flux. This strongly increases during the decline (see also Fig. 4). The final panel shows the inferred inner radius of the disc. This remains remarkably constant in this model at around $10 R_g$ (see also Fig. 2), corresponding to $\sim 30 R_g$ after a colour temperature correction. This lack of change in the inner disc radius is in conflict with the truncated disc model predictions that the change in spectral hardness (see second panel) is driven by changes in the solid angle subtended by the disc to the hard X-ray source. If instead there is a separate soft X-ray component (see Fig. 8) as required in the similarly dim low/hard state spectra from XTE J1118+480 then these data © 2009 RAS, MNRAS 000, 1–11

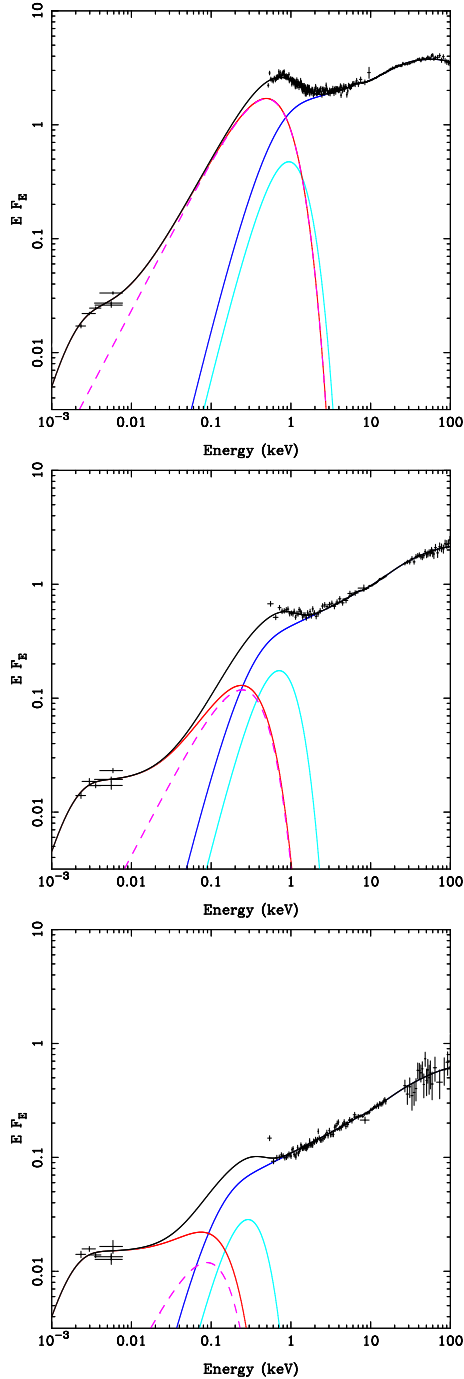


Figure 7. The same 3 spectra (10, 20 and 30) as in Fig. 3, fit with the irradiated disc model and corrected (data and model) for absorption. The magenta dashed line is the intrinsic disc emission, the red line includes irradiation of the outer disc, and the cyan line shows the additional flux from irradiation of the inner disc. The Comptonised emission and its reflected spectrum are shown in blue. While the inner disc irradiation, f_{in} , drops, the increase in L_c/L_d means that the total disc spectrum is more distorted by irradiation at lower fluxes.

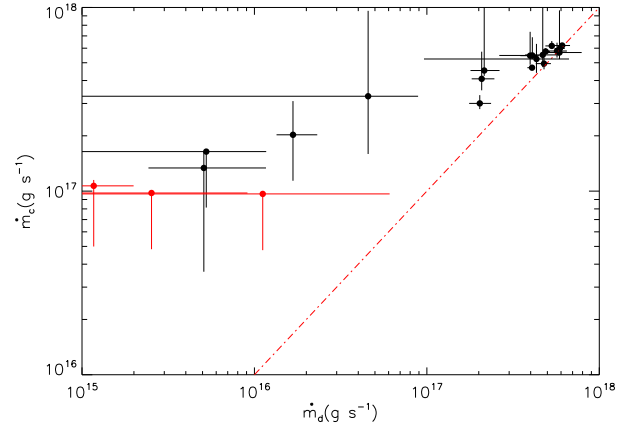


Figure 8. Irradiated disc model mass accretion rate through the disc, \dot{m}_d versus that through the corona, \dot{m}_c , derived from $(L_c/L_d)(R_d/R_c)\dot{m}_d$, with $R_c = 3.5 R_g$ fixed by requiring $\dot{m}_c \approx \dot{m}_d$ (shown by the red dashed line) for the brightest spectra. The red points show the 3 faintest spectra where there is no significant additional soft X-ray component. Even without these spectra the trend is clear that \dot{m}_c gets progressively larger than \dot{m}_d as the source declines. This is opposite to the expected trend from a radiatively inefficient flow. are away from the line.

The spectral fitting parameters give L_c/L_d , \dot{m}_d and R_d . Close to the peak of the outburst, even a radiatively inefficient flow should have $\eta_{corona}/\eta_{disc} \sim 1$. Here we also expect $\dot{m}_c \sim \dot{m}_d$, which requires R_c to be around 3 times smaller than R_d at this point. We can then calculate \dot{m}_c assuming $\eta_{corona}/\eta_{disc}$ and R_c remain constant. This is plotted against \dot{m}_d in Fig. 8. The red line is $\dot{m}_c = \dot{m}_d$, showing clearly that these models favour a larger mass accretion rate through the corona than through the disc on the decline. This conclusion is strengthened if the flow is increasingly radiatively inefficient at lower mass accretion rates, as the observed X-ray flux would then require an even larger coronal mass accretion rate to power the same amount of hard X-ray emission.

This conclusion is driven by the *observational* requirement for a soft X-ray component in the late state decline data. This is weak, but significantly present in all but the last three datasets (assuming that the absorption column remains constant: Cabanac et al. 2009). It combines a low luminosity with a fairly high (soft X-ray) temperature, which leads to the derived small radius and low mass accretion rate. This low mass accretion rate is then much smaller than that required to power the observed hard X-ray emission.

We illustrate this by re-coding the irradiated disc model to force $\dot{m}_c = \dot{m}_d$ for $\eta_{corona}/\eta_{disc} = 1$. This forces the disc to have a higher mass accretion rate, so it must truncate at a larger radius so as not to overproduce the observed soft X-ray component. Irradiation of the inner disc should then be negligible, so we fix $f_{in} = 0$ for physical consistency, and we focus first on the X-ray data alone so we also fix $f_{out} = 0$.

We fit this to spectrum 24 (the lowest luminosity data for which the disc is significantly detected in the soft X-ray flux), and first focus on the X-ray data alone. The mass accretion rate through the disc is much higher ($1.2 \pm 0.1 \times 10^{17}$ g/s compared to 1.0×10^{16} in the `diskir` fits) and the disc inner radius increases to $30 R_g$ from $\sim 5 R_g$ (i.e. $90 R_g$ and $15 R_g$ after a colour temperature correction). This disc contributes to the spectrum only at the softest energies of the *Swift* XRT, and its sharp rise is rather different to the more gradual curvature seen in the soft X-ray emission. Thus

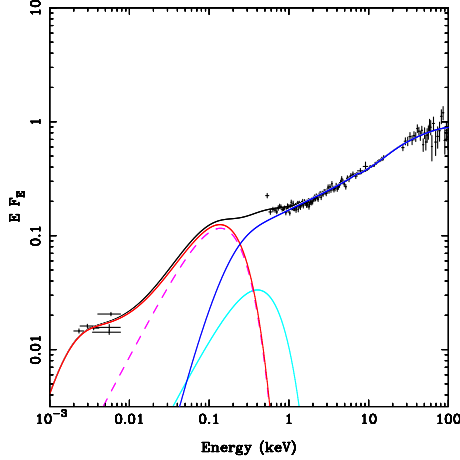


Figure 9. Spectrum 24 fit by a model where $\dot{m}_d = \dot{m}_c$ and a separate component (cyan, modelled with `diskbb`) to fit the soft X-ray emission. The observed strong X-ray flux requires a large mass accretion rate through the disc, so this has to truncate at $\sim 50 R_g$, forming the UV peak, so as not to overproduce the soft X-ray emission.

this gives a significantly worse fit ($\chi^2_\nu = 626/632$ versus $600/630$, where the two extra free parameters are L_c/L_d and f_{in}). We can only recover the same quality of fit with $\dot{m}_d = \dot{m}_c$ by including an additional soft component. This allows the disc to recede back even further, to $\sim 50 R_g$ (i.e. $\sim 150 R_g$), so that the truncated disc makes no contribution to the soft X-ray flux. Fig. 9 shows this fit including now the optical/UV data with $f_{out} = 2 \times 10^{-3}$ (similar to that derived from the original fits, see Fig. 6).

Irradiation can make such a hot, weak component if the irradiated disc area is *small*. We fixed the radius of the reprocessing region at $1.1 \times R_d$ for the fits in Fig. 6, but as the disc recedes then the changing geometry means that this should also drop. We allow this to be a free parameter with $\dot{m}_c = \dot{m}_d$ and can recover as good a fit as before ($\chi^2_\nu = 601/632$) with ~ 1 per cent of the bolometric flux being reprocessed in a region with $R_{irr} = 1.002 R_d$. However, illumination of such a tiny area of the disc surface seems unreasonable from illumination by a central source.

5 ORIGIN OF SOFT X-RAY COMPONENT

5.1 Outburst Peak

The soft X-ray component seen at the peak of the hard state during the outburst of SWIFT J1753.5-0127 is clearly from the disc. While the system parameters are rather poorly known, the radii derived close to the peak are $\sim 15 R_g$, corresponding to $\sim 45 R_g$ after a colour temperature correction. This is consistent with the disc being recessed back from the last stable orbit, as required for the truncated disc/hot inner flow interpretation of the hard state. There are two independent lines of support for this number. The first comes from the fact that the hard X-ray spectrum is softer close to the peak, clearly consistent with the disc providing an increasing source of seed photons to Compton cool the hot X-ray plasma. Since most of the gravitational potential energy to power this corona is concentrated within $20 R_g$ then it seems most likely that the disc extends down to similarly small radii. This means that there can also be irradiation of the inner disc by the hard X-ray emission, leading to reflection and thermalisation of the incident

flux. We see evidence for both these processes in the spectrum, with the extra flux from irradiation increasing the inferred disc radius from the value of $\sim 11 R_g$ inferred from the simple (unirradiated) disc fits to the X-ray spectrum, to $15 R_g$ (i.e. from 30 to $45 R_g$ after colour temperature correction). The second is from low frequency QPO which is at its maximum of ~ 0.8 Hz in these data. This implies an outer radius of $\sim 20 - 30 R_g$ assuming that the QPO is produced by Lense-Thirring (vertical) precession of the hot flow around a $10 M_\odot$ black hole (Ingram, Done & Fragile 2009).

The mass accretion rate required to power the disc emission is comparable with that required to power the coronal hard X-ray emission assuming that the corona extends down to a radius which is ~ 5 times smaller than that of the disc i.e. $3.5 R_g$ for the parameters assumed here, i.e. $\sim 9 R_g$ with a colour temperature correction. We stress again that these system parameters are poorly known, though this appears quite reasonable. Much smaller radii could be potentially feasible for a hot inner flow, irrespective of the spin of the black hole, as numerical simulations of the MRI turbulence show that the large scale height magnetic fields can extract energy from the infalling material beyond the last stable orbit (e.g. Krolik, Hawley & Hirose 2005).

5.2 Late Stage Decline

The outburst peak spectra then form a template for comparison with the later stages of the decline, where the bolometric flux is lower by a factor 10. The truncated disc/hot inner flow model makes a clear prediction that these should have a larger inner disc radius, decreasing the importance of illumination on the inner edge of the disc, and decreasing the amount of associated reflection. Thus illumination of the surface of the disc is not expected to be important in distorting the derived inner disc radii in these spectra. Similarly, as there is little (or no) overlap in radii between the hot inner flow and disc, so the disc emission cannot be strongly suppressed by Comptonisation as can be the case close to the transition (Kubota & Done 2004; Makishima et al. 2008). Thus any disc component seen in these spectra should give a fairly unbiased view of the inner radius of the flow. Yet associating the observed soft X-ray component with this disc gives derived radii which are as small, if not smaller than, the radii seen at the outburst peak, in clear conflict with the truncated disc models (see Figs 4 and 6).

However, these radii are themselves in more subtle conflict with the observations. The small disc has very small luminosity compared to the coronal emission. This requires that the coronal mass accretion rate must be large compared to that through the disc if the corona is powered by matter accreting through it. Thus the corona cannot be predominantly fed by material evaporating from the inner edge of the disc, but instead requires a completely separate coronal flow which incorporates most of the incoming mass accretion from the companion star. Yet it seems quite unlikely that the incoming cool Roche lobe overflow stream would be able to form such a coronal flow at large radii.

Instead it seems more feasible that the corona is *not* powered by its own mass accretion supply, as in the truncated disc models, but is instead powered by mass accreted through the disc, but whose energy is released in the corona (e.g. Svensson & Zdziarski 1994). However, this model itself runs into difficulties since the simplest idea would be for magnetic buoyancy to transport the energy vertically. The energy is then released in a corona above the disc, so the corona is co-spatial with it and illuminates it. This gives rise to a reprocessed luminosity $L_{rep} = \frac{1}{2}(1-a)L_c$ (where a is the albedo, and the factor $\frac{1}{2}$ assumes the corona emits isotropically) adds to the

intrinsic disc luminosity (Haardt & Marashi 1993). For hard spectra, such as those observed here, the reflection albedo $a < 0.3$, hence the disc flux should be at least $L_c/3$. Yet we observe a disc flux of $\leq L_c/20$ towards the end of the outburst. Thus the only way to circumvent the reprocessing limits whilst having all the mass accrete via the disc is if the energy is advected radially as well as vertically. Then it can be released in a more centrally concentrated region, on size scales smaller than the (small!) disc inner radius. The alternative of having the hard X-rays be strongly beamed away from the disc, is ruled out by the very similar dim low/hard state spectra seen in XTE J1118+480 (Frontera et al. 2001; 2003; Reis, Miller & Fabian 2009), which has high inclination ($\geq 70^\circ$) so that we must see a similar hard X-ray flux to that of the disc.

A potentially less arbitrary solution than using magnetic fields to transport the energy in a dissipationless fashion is if the observed soft X-ray component in the late stages of the decline is not from the disc. The spectra clearly show that the observed soft X-ray emission cannot produce the optical/UV emission without a large change in the reprocessed fraction in the outer disc from that seen during the outburst peak. Yet the outburst remained in the low/hard state, so there is no expected change in source geometry, so the fraction of the total flux which illuminates the outer disc should not change dramatically. Similarly, there is no large change in spectral shape which might produce such a large difference in thermalisation fraction. Yet the observed soft X-ray component is a factor 10 further below the UV emission than at the outburst peak (Fig. 5). This could be used to argue that the real disc is truncated, as in Fig. 7, so is larger and cooler, so that the same amount of reprocessing can produce the optical/UV.

However, it is clear that the optical/UV emission does change character during the decline. The rapid variability of the optical flux changes dramatically during the decline, switching to an anti-correlation of the optical and X-ray emission (Hynes et al. 2009). Clearly this shows that the optical is no longer made predominantly by reprocessing of the hard X-ray flux, so it gives only an upper limit to the irradiated disc flux.

Thus the optical emission does not trace the outer disc, so cannot constrain our inner disc models. Instead, we use the similarly dim low/hard state spectra from XTE J1118+480 to argue for a non-disc origin for the soft X-ray component. This object has an absorption column which is an order of magnitude lower than that to SWIFT J1753.5-0127. This gives a correspondingly more sensitive view of the UV and soft X-ray emission, where it is clear that there is a large, cool disc seen in the UV and EUV bandpass (Esin et al. 2001; McClintock et al. 2001) which is completely inconsistent in luminosity and temperature with the much weaker, higher temperature 'disc' emission seen in soft X-rays (Frontera et al. 2001; 2003; Reis, Miller & Fabian 2009). There are plainly *two* components in this source, one which is consistent with a truncated disc, making no impact on the soft X-ray emission, *and* another component which produces weak soft X-ray flux. This is very similar to the spectrum of 24 as shown in Fig. 9.

Thus for the late stage decline, our modeling with an irradiated disc is not supported by the data. The cross-correlation of the rapid variability clearly shows that the optical/UV cannot be made by reprocessing in the outer disc, while XTE J1118+480 clearly shows that the soft X-rays form a separate component to the observed UV/EUV emission from the (truncated!) disc. What then produces the observed soft X-ray component, and what produces the observed optical/UV emission?

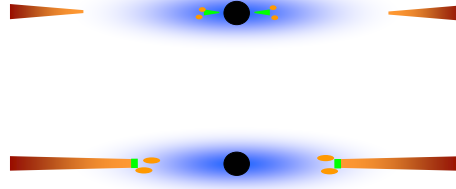


Figure 10. Two potential geometries for a soft X-ray component (highlighted in green) from a small area, with short timescale variability dominated by reprocessing of the hard X-rays, and additional variability at longer timescales. With irradiation of a residual inner disc, the small area implies a small radial extent. Conversely, with irradiation of the inner rim of a large radius truncated disc, a small area implies a small vertical extent. Additional long timescale variability can be generated at the disc outer or inner edge, respectively, by clumping or turbulence.

6 ORIGIN OF THE SOFT X-RAY COMPONENT DURING THE DECLINE

SWIFT J1753.5-0127 was observed by *XMM-Newton* in March 2006 i.e. after the end of the first intensive SWIFT campaign covering the outburst decline. These data are analysed by Wilkinson & Uttley (2009), and have much better signal-to-noise than those of the late decline *SWIFT* spectra, but are very similar in shape and intensity. The higher statistics in these data mean that the soft component is *unambiguously* detected, at very high significance. The same spectra model as used in Table 1 (DISKBB+THCOMP with absorption fixed at $0.2 \times 10^{22} \text{ cm}^{-2}$) gives $kT_{disc} = 0.25 \pm 0.01 \text{ keV}$ and norm of 1080 ± 100 .

The timing analysis of Wilkinson & Uttley (2009) showed that this soft X-ray component variability strongly correlates with the hard X-ray variability on short timescales i.e. is driven by reprocessing. However, on longer timescales, there is additional variability in the soft X-ray flux, implying that there are intrinsic fluctuations in the disc emission as well. The result that much of the short term variability correlates with the hard X-rays rules out a completely separate soft X-ray component such as the jet, while the additional soft X-ray variability shows that the component is truly separate as opposed to being produced from continuum curvature of the X-ray emission or reflection (suggested by Hiemstra et al. 2009 as a potential origin for the soft X-rays). These variability constraints mean that there are only two potential origins for the soft X-ray component which arises from a small area with relatively high temperature. Firstly, this could be emission from the surface of a residual inner disc, forming a small ring from the last stable orbit to some (small) outer radius. Secondly, this could be the inner face of a truncated disc. We sketch these two possibilities in Fig. 10, and outline them below.

6.1 Irradiation of a residual inner disc

Evaporation of the disc by thermal conduction is a plausible mechanism to form a truncated disc/ hot inner flow geometry (e.g. Liu et al. 1999). Counterintuitively, this is not most efficient at the smallest radii, as these also have the highest coronal densities, so have the highest condensation rates. Evaporation first erodes a *gap* in the disc, leaving a residual inner disc. This gap expands radially, eventually giving a fully truncated disc if the mass accretion rate is low enough (Mayer & Pringle 2007). However, close to the transition, the residual disc can remain. This geometry allows the outer

disc to carry all the mass accretion rate. This disc evaporates into a corona, truncating it at some large radius into a coronal flow which carries all the mass accretion rate. However, as the flow accretes to smaller radii, the increasing density gives an increasing condensation rate and some small fraction of the material can condense out of the hot flow. This forms a cool ring at the innermost radii, with a mass accretion rate which is only a small fraction of the total mass accretion rate, with the rest of the material accreting via the coronal flow (Liu & Meyer-Hofmeister 2001).

Reprocessing is still an issue, but if the ring is small, extending over a very narrow range of radii, then it does not subtend a large solid angle to the coronal X-ray emission, so could potentially produce the large observed ratio of coronal to (inner) disc luminosity. Some reprocessing is *required* in order to produce the short term variability, but there could also be intrinsic variability in the extent of this residual disc.

6.2 Irradiation of the inner face of a truncated disc

The temperature of the irradiated region is required to be substantially hotter than that of the disc itself, requiring a very small reprocessing area. This seems very unlikely for a central source illuminating the top/bottom surface of thin disc. However, the disc has some (small) half thickness, H_d , so its inner rim forms a distinct, small area $\approx 4\pi R_d H_d$ and subtends a solid angle $\approx H_d/R_d \times 4\pi$ to the central source. The small reprocessing area found in section 4.2 above corresponds to $H_d/R_d \sim 0.004$, predicting $f_{in} = (1 - a)H_d/R_d \approx 0.002$, where a is the reflection albedo. This is a factor 5 smaller than f_{in} derived from the data, but potentially feasible given the large uncertainties both on the parameters and on the modeling.

The irradiation origin then gives directly the rapid variability, while turbulence caused by clumping instabilities on this edge could give the required longer term additional variability.

7 ORIGIN OF OPTICAL/UV EMISSION DURING THE DECLINE

As noted by Motch et al. (1985) in GX339-4, the X-ray emission in the dim low/hard state can extrapolate back quite accurately to fit the optical spectrum (see also Corbel & Fender 2002; Nowak 2005). One way to produce this is via a single synchrotron component from the innermost post-shock region of the jet. This is self absorbed in the IR, strongly suppressing the emission at lower frequencies. As the jet stretches out, each part of it produces a synchrotron component which peaks at a lower frequency than those closer to the center. All of these make the flat spectrum seen in the radio (e.g. Markoff & Nowak 2005; Maitra et al. 2009). However, the non-thermal synchrotron makes the optical and X-ray emission from a single scattering in a single region, so it is hard to see how this can make the weak anti-correlation between the optical and X-ray flux with lead of a few hundred milliseconds which seems typical of this state (Motch et al. 1985; Kanbach et al. 2001; Gandhi et al. 2008; Durant et al. 2008).

Conversely, the cross-correlation signal *can* be explained if the optical emission is from the jet, while the X-ray emission is from the corona (Malzac, Merloni & Fabian 2004). However, the close match of the optical and X-ray spectra is then very unexpected if these are really from different components.

Instead, if the spectrum is formed from thermal Comptonisation from self-produced cyclo-synchrotron photons in the hot

flow then there can be complex time variability properties imprinted via propagating fluctuations through an inhomogeneous flow (Kotov, Churazov & Gilfanov 2001; Arévalo & Uttley 2006). Whether these can indeed explain the anti-correlation between optical and X-ray by such spectral pivoting (Körding & Falcke 2004) remains to be seen.

8 CONCLUSIONS

The combined *Swift* and *RXTE* observations from the black hole transient SWIFT J1753.5-0127 give one of the best datasets to probe the evolution of the inner edge of the accretion disc in the low/hard state. These instruments cover the optical/UV and soft/hard X-ray bandpasses, giving a detailed picture of the spectral evolution during the low/hard state outburst.

We fit these with a sophisticated irradiated disc model and find that this gives a self-consistent picture around the outburst peak. Weak irradiation increases the inferred radius of the inner disc by a factor ~ 1.5 . Photons from the disc are the seeds for Compton upscattering to produce the hard X-ray emission, and this hard X-ray emission weakly illuminates the outer disc to produce the observed optical/UV by reprocessing, as confirmed by the optical/X-ray cross-correlation (Hynes et al. 2009).

However, we find clear evidence that the model breaks down as the source flux declines. The optical spectra require increasingly unlikely levels of reprocessing to explain the observed emission. A change in origin of the optical emission is confirmed by the dramatic change in optical/X-ray cross-correlation signal (Hynes et al. 2009). While the cross-correlation can be explained in models where the optical is produced by the jet and the X-rays in a corona (Malzac, Merloni & Fabian 2004), this does not explain the excellent match between the optical and X-ray spectra. Instead it seems more likely that there is a single component connecting the optical and X-ray spectra. The complex cross-correlation then remains an issue especially for a single synchrotron component from the jet, but it may potentially be explained by thermal Comptonisation of IR cyclo-synchrotron emission in an inhomogeneous hot flow.

More fundamentally for the focus of this paper, the soft X-ray emission during the decline may not be thermal emission from the disc either. If it is, its radius does not change markedly from that seen at the outburst peak, in clear conflict with the predictions of the truncated disc model. But it also implies that the mass accreting through the disc is much less than the mass accretion rate required to power the corona. Yet it seems most likely that the mass does accrete through the outer disc, in which case the observed weak soft X-ray disc emission is a problem. Either the mass accretes through the disc but most of the energy is transported vertically *and* radially (to get around the reprocessing limits) by magnetic fields to power a small, central hard X-ray corona, or the soft X-rays are from an additional component, with the truncated disc peaking in the UV.

The lower absorption to XTE J1118+480 allows us to distinguish between these possibilities. Here, we can see a cool component peaking in the UV which is clearly distinct from the soft X-ray emission. The UV component fits well to a cool disc, truncated at large radii, so the soft X-ray component cannot be the same material. This may still be associated with the inner disc, perhaps from irradiation of its inner rim, or via a residual inner disc in the discontinuous disc geometry predicted by evaporation models (e.g. Liu & Meyer-Hofmeister 2001). However, it is also possible that the soft X-rays are instead produced in a completely different way, such as ionised reflection from grazing incidence angle illumina-

tion of the outer disc. Whatever their origin, it is clear from XTE J1118+480 that the weak soft X-ray component seen in the dim low/hard state does not trace the inner edge of the disc, so cannot be used to constrain the truncated disc models.

ACKNOWLEDGEMENTS

CYC and CD would like to thank Kim Page for help in extracting the *Swift* XRT data.

REFERENCES

- Arévalo P., Uttley P., 2006, *MNRAS*, 367, 801
- Cabanac C., Fender R. P., Dunn R. J. H., Körding E. G., 2009, *MNRAS*, 396, 1415
- Cadolle Bel M., Ribó M., Rodríguez J., Chaty S., Corbel S., Goldwurm A., Frontera F., Farinelli R., D’Avanzo P., Tarana A., Ubertini P., Laurent P., Goldoni P., Mirabel I. F., 2007, *ApJ*, 659, 549
- Corbel S., Fender R. P., 2002, *ApJ*, 573, L35
- De Matteo T., Celotti A., Fabian A. C., 1997, *MNRAS*, 291, 805
- Done C., Gierliński M., 2003, *MNRAS*, 342, 1041
- Done C., Gierliński M., Kubota A., 2007, *A&ARv*, 15, 1 (DGK07)
- Dunn R. J. H., Fender R. P., Körding E. G., Belloni T., Cabanac C., 2009, *MNRAS*, submitted
- Durant M., Gandhi P., Shahbaz T., Fabian A. P., Miller J., Dhillon V. S., Marsh T. R., 2008, *ApJ*, 682, L45
- Esin A. A., McClintock J. E., Drake J. J., Garcia M. R., Haswell C. A., Hynes R. I., Munro M. P., 2001, *ApJ*, 555, 483
- Esin A. A., McClintock J. E., Narayan R., 1997, *ApJ*, 489, 865
- Fender R. P., Belloni T. M., Gallo E., 2004, *MNRAS*, 355, 1105
- Fender R., Garrington S., Muxlow T., 2005, *ATel*, 558, 1
- Fender R. P., Homan J., Belloni T. M., 2009, *MNRAS*, 396, 1370
- Frontera F., Zdziarski A. A., Amati L., Mikolajewska J., Belloni T., Del Sordo S., Haardt F., Kuulkers E., Masetti N., Orlandini M., Palazzi E., Parmar A. N., Remillard R. A., Santangelo A., Stella L., 2001, *ApJ*, 561, 1006
- Frontera F., Amati L., Zdziarski A. A., Belloni T., Del Sordo S., Masetti N., Orlandini M., Palazzi E., 2003, *ApJ*, 592, 1110
- Gallo E., Migliari S., Markoff S., Tomsick J. A., Bailyn C. D., Berta S., Fender R., Miller-Jones J. C. A., 2007, *ApJ*, 670, 600
- Gandhi P., Makishima K., Durant M., Fabian A. C., Dhillon V. S., Marsh T. R., Miller J. M., Shahbaz T., Spruit H. C., 2008, *MNRAS*, 390, L29
- Gierliński M., Done C., Page K., 2008, *MNRAS*, 388, 753 (GDP08)
- Gierliński M., Done C., Page K., 2009, *MNRAS*, 392, 1106 (GDP09)
- Haardt F., Maraschi L., 1993, *ApJ*, 413, 507
- Hiemstra B., Soleri P., Méndez M., Belloni T., Mostafa R., Wijmands R., 2009, *MNRAS*, 394, 2080
- Hjellming R. M., Han X., 1995, *xrbi.nasa*, 308
- Hynes R. I., Mauche C. W., Haswell C. A., Shrader C. R., Cui W., Chaty S., 2000, *MNRAS*, 539, L37
- Hynes R. I., O’Brien K., Mullally F., Ashcraft T., 2009, *MNRAS*, 399, 281
- Ingram A., Done C., Fragile P. C., 2009, *MNRAS*, 397, L101
- Jimenez-Garate M. A., Raymond J. C., Liedahl D. A., 2002, *ApJ*, 581, 1297
- Kanbach G., Straubmeier C., Spruit H. C., Belloni T., 2001, *Nature*, 414, 180
- King A. R., Ritter H., 1998, *MNRAS*, 293, 42
- Körding E., Falcke H., 2004, *A&A*, 414, 795
- Kotov O., Churazov E., Gilfanov M., 2001, *MNRAS*, 327, 799
- Krolik J. H., Hawley J. F., Hirose S., 2005, *ApJ*, 622, 1008
- Kubota A., Done C., 2004, *MNRAS*, 353, 980
- Kubota A., Makishima K., Ebisawa K., *ApJ*, 560, 147
- Lasota J. P., 2001, *NewAR*, 45, 449
- Liu B. F., Meyer-Hofmeister E., 2001, *A&A*, 372, 386
- Liu B. F., Yuan W., Meyer F., Meyer-Hofmeister E., Xie G. Z., 1999, *ApJ*, 527, L17
- Maitra D., Markoff S., Brocksopp C., Noble M., Nowak M., Wilms J., 2009, *MNRAS*, in press, (arXiv:0904.2128)
- Makishima K., Takahashi H., Yamada S., Done C., Kubota A., Dotani T., Ebisawa K., Itoh T., Kitamoto S., Negoro H., Ueda Y., Yamaoka K., 2008, *PASJ*, 60, 585
- Malzac J., Merloni A., Fabian A. C., 2004, *MNRAS*, 351, 253
- Markoff S., Falcke H., Fender R., 2001, *A&A*, 372, L25
- Markoff S., Nowak M. A., 2005, *ApJ*, 635, 1203
- Mayer M., Pringle J. E., 2007, *MNRAS*, 376, 435
- McClintock J. E., Haswell C. A., Garcia M. R., Drake J. J., Hynes R. I., Marshall H. L., Munro M. P., Chaty S., Garnavich P. M., Groot P. J., Lewin W. H. G., Mauche C. W., Miller J. M., Pooley G. G., Shrader C. R., Vrtilik S. D., 2001, *ApJ*, 555, 477
- McClintock J. E., Remillard R. A., 2006, in: *Compact stellar X-ray sources*. W. Lewin, M. van der Klis (Eds.). Cambridge Astrophysics Series, No. 39, Cambridge University Press, 157
- Mitsuda, K., Inoue, H., Koyama, K., Makishima, K., Matsuoka, M., Ogawara, Y., Suzuki, K., Tanaka, Y., Shibazaki, N., Hirano, T., 1984, *PASJ*, 36, 741
- Motch C., Ilovaisky S. A., Chevalier C., Angebault P., 1985, *SSRv*, 40, 219
- Narayan R., Yi I., 1995, *ApJ*, 452, 710
- Niedźwiecki A., 2005, *MNRAS*, 356, 913
- Nowak M., 2005, *Ap&SS*, 300, 159
- Poutanen J., Krolik J. H., Ryde F., 1997, *MNRAS*, 292, L21
- Reis R. C., Miller J. M., Fabian A. C., 2009, *MNRAS*, 395, L52
- Russell D. M., Fender R. P., Hynes R. I., Brocksopp C., Homan J., Jonker P. G., Buxton M. M., 2006, *MNRAS*, 371, 1334
- Shapiro S. L., Lightman A. P., Eardley D. M., 1976, *ApJ*, 204, 187
- Shahbaz T., van der Hoof F., Casares J., Charles P. A., van Paradijs J., 1998, *MNRAS*, 306, 89
- Shakura N. I., Syunyaev R. A., 1973, *A&A*, 24, 337
- Shrader C.R., Titarchuk L., 1999, *ApJ*, 521, L121
- Svensson R., Zdziarski A. A., 1994, *ApJ*, 436, 599
- van Paradijs J., 1996, *ApJ*, 464:L139+
- Wardziński G., Zdziarski A. A., 2000, *MNRAS*, 314, 183
- Wilkinson T., Uttley P., 2009, *MNRAS*, 397, 666
- Zdziarski A. A., Poutanen J., Johnson W. N., *ApJ*, 542, 703
- Zombeck M. V., 1990, *Handbook of space astronomy and astrophysics*. Cambridge Univ. Press, Cambridge
- Zurita C., Durant M., Torres M. A. P., Shahbaz T., Casares J., Steeghs D., 2008, *ApJ*, 681, 1458
- Życki P. T., Done C., Smith D. A., 1999, *MNRAS*, 305, 231